

Use of Geoelectrical Resistivity to Delineate the Seawater Intrusion in the Northwestern Part of the Nile Delta, Egypt



Zenhom E. Salem and Osman M. Osman

Abstract Mapping of the boundaries between freshwater and saltwater was helpful in surface resistivity surveys because of the high electric conductivity of saltwater relative to freshwater. A total of 30 electrical soundings were measured to configurate the seawater intrusion. Accordingly, two zones of groundwater quality were delineated: the slightly freshwater zone in the southern part, with resistivity range of 15–90 Ω m, and the brackish water to saltwater zone, with a very low resistivity of <2 Ω m in the northwestern parts. In addition to tracing the freshwater-seawater contact zone, three geoelectric layers were detected. The surface layer composed of sand, clay, and silt. Its resistivity ranges from 5 to 512 Ω , and the thickness varies from 1 to 25 m. The aquifer layer is composed of sand with intercalations of clay with resistivity ranging from 15 to 90 Ω m and thickness from 25 to 120 m. The clay layer resistivity ranges from 2 to 15 Ω m and thickness from 2 to 69 m.

Keywords Geoelectrical resistivity, Northwestern Nile Delta, Quaternary aquifer, Seawater intrusion

Contents

1	Introduction	426
2	Description of the Study Area	427
3	Methodology	431
3.1	Data Acquisition (Field Work)	433
3.2	Data Processing	433
3.3	Data Interpretation	434

Z.E. Salem (✉)

Geology Department, Faculty of Science, Tanta University, Tanta, Egypt

e-mail: zenhomsalem@yahoo.com

O.M. Osman

Geology Department, Faculty of Science, Damanshour University, Damanshour, Egypt

A. M. Negm (ed.), *Groundwater in the Nile Delta*,

Hdb Env Chem (2019) 73: 425–460, DOI 10.1007/698_2017_175,

© Springer International Publishing AG 2017, Published online: 14 December 2017

4	Results and Discussion	435
4.1	Resistivity Spectrum	435
4.2	Geoelectrical Cross Sections	435
4.3	Geoelectrical Maps	449
4.4	3D Resistivity Model	452
5	Conclusions	454
6	Recommendations	456
	References	456

1 Introduction

Coastal regions are of incredible ecological, economic, and social importance. Hence, the execution of reasonable observing and insurance activities is basic for their safeguarding and for guaranteeing future utilization of this asset [1]. Post [2] has characterized the coastal aquifers as the subsurface reciprocals of seaside zones where mainland new groundwater and seawater meet. Seaside fields are frequently polluted by saltwaters, and the procedure related to the marine water entering an aquifer is for the most part called seawater intrusion. Seawater intrusion becomes a severe problem in arid and semiarid regions where the groundwater constitutes the main freshwater resource. Mixing of only 3% seawater with freshwater in a coastal aquifer would render the freshwater resource unsuitable for human consumption [3, 4]. Seawater intrusion is regarded as a natural process that might be accelerated or retarded by external factors such as the increase or decrease in the groundwater pumping, irrigation system, recharge rates, land use, and possible seawater rise due to the impact of global warming [3]. Diverse methodologies have been received to evaluate seawater intrusion. For instance, many studies including Wilson et al. [5], Diab and Saleh [6], Sherif et al. [7–9], Diab et al. [10], Petalas and Diamantis [11], Sherif [12], Polemio et al. [13], Petalas and Lambrakis [14], Somay and Gemici [15], Salem et al. [16], Salem and El-horiny [17], Sefelnasr and Sherif [18], and Salem and Osman [19] have utilized geochemical strategies in view of modeling technique, stable isotopes, and hydrochemical data to evaluate the seawater intrusion.

Werner et al. [20] stated that the field of coastal hydrogeology, considered as a subdiscipline of hydrogeology, spans seawater intrusion, submarine groundwater discharge (SGD), beach-scale hydrology, sub-seafloor hydrogeology, and studies on geological time scales involving coastline geomorphology. Despite this, coastal aquifer hydrodynamics and seawater intrusion remain challenging to measure and quantify, commonly used models and field data are difficult to reconcile, and predictions of future coastal aquifer functioning are relatively uncertain across both regional and local (individual well) scales. The extent of seawater intrusion into the fresh groundwater is affected by subsurface geology, hydraulic gradient, rate of groundwater recharge, and groundwater pumping amounts [21]. Investigating the geometry of seawater intrusion extent, utilization of data from geological research, groundwater geochemistry, well drilling, and exploitation boreholes are used. These strategies are costly and tedious, keeping their utilization on an

expansive scale. Interestingly, geophysical measurements can give a more affordable approach to enhance the information of an arrangement of boreholes [22]. Geophysical prospecting strategies can give corresponding information that empower geological correlations, even in areas where there are no information from boreholes. Indirect geophysical strategies (like electrical resistivity tomography (ERT) and VES survey) create continuous information throughout a given profile. It helps in understanding spatial relations between fresh and seawater which normally coincide in beach front aquifers [23].

Recently, geophysical methods (especially the direct current resistivity) are considered as major tools for solving the complicated hydrogeological and environmental problems especially in the coastal areas, e.g., Steeples [24], Lapenna et al. [25], Pantelis et al. [26], Chianese and Lapenna [27], and Naudet et al. [28]. Electrical resistivity method was used by many authors around the world to characterize the coastal areas; among them are Urish and Frohlich [29], Ebraheem et al. [30], Kruse et al. [31], Nowroozi et al. [32], Abdul Nassir et al. [33], Balia et al. [34], Choudhury and Saha [35], Batayneh [36], Bauer et al. [37] Khalil [38], Sherif et al. [39], Koukadaki et al. [40], Cimino et al. [41], Satriani et al. [1], and Fadili et al. [42].

In addition to surface contaminants [43], the groundwater quality in the Nile Delta is affected mainly by seawater intrusion [30, 44–47]. In the last decades, a common problem of Nile Delta sandy aquifer is the degradation of the groundwater quality due to seawater intrusion from the north and excessive pumping in relation to average natural recharge [48]. A detailed review of seawater intrusion in the Nile Delta groundwater system and the basis for assessing impacts due to climate changes and water resources development was discussed in Mabrouk et al. [49]. The encountered recent studies that used electrical resistivity to delineate the seawater–freshwater relationship in the northern part of the Nile delta are Attwa et al. [50], Mohamed [51], Salem et al. [3], and Tarabees and El-Qady [52]. The subsurface thermal regime was also used to trace the seawater intrusion in the Nile Delta [16, 53].

The purpose of this chapter is to present a detailed vertical electrical sounding survey in the proposed area of the Nile Delta aquifer to delineate and follow the seawater intrusion of the study area located in the northwestern part of the Nile Delta (Fig. 1). The interpretation includes the correlation of these similar or nearly similar parameters to illustrate the vertical, horizontal, and lateral extent of the seawater intrusion as well as the subsurface geologic structural configuration. This study supplies the decision maker with information for groundwater management strategy.

2 Description of the Study Area

The west of the Nile Delta represents one of the largest groundwater provinces in northern Egypt. Groundwater occurrence and distribution are governed by the geographic location, the sedimentary sequence, the geologic structure, and the

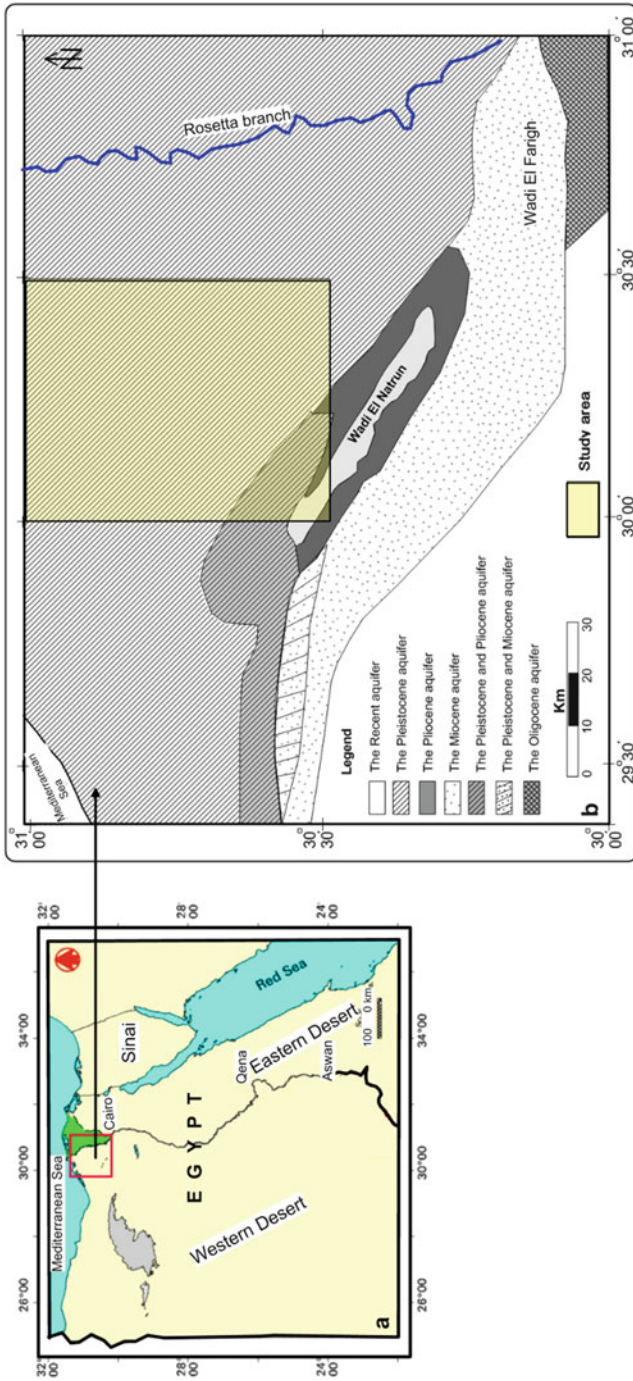


Fig. 1 Maps show the location of the study area (a) and describe its hydrogeology (b)

physiographic features. The study of groundwater is very important to detect the flow direction and saltwater intrusion as well as to ensure its quality for several purposes. The area is located to the west of the Nile Delta in northern Egypt (Fig. 1). It is bounded geographically by latitudes $30^{\circ} 30'$ and $31^{\circ} 00'$ N and longitudes $30^{\circ} 00'$ and $30^{\circ} 30'$ E. The study area is characterized by many human activities such as agricultural, industrial, and desert land reclamation. The reclamation processes are increased in the past decades, so the land uses are changed [54]. Over the years, agricultural areas have begun to move from the fertile soils of the Nile River to the east [19]. While most fields are irrigated by water from the Nile, high water tables have allowed the use of groundwater to support additional vegetable crops.

The sedimentary succession in the western Nile Delta reached up to 4 km in thickness and ranged in age from Triassic to Quaternary. The surface deposits of the West Nile Delta (Fig. 1b) are of Oligocene, Miocene, Pliocene, and Quaternary ages. The Oligocene rocks are portrayed by ferruginous sandstone and sands and sometimes gravels. These deposits are covered by some dissected basaltic sheet and located in the southern part of the West Nile Delta (Fig. 1b). Miocene deposits (Moghra Formation, Moghra aquifer) are up to 200 m in thickness and made out of shallow marine intercalations. Sediments are unconformably overlain the Miocene deposits. The Pliocene is portrayed by estuarine clayey facies at the base and fluvio-marine and shallow marine white limestones at the top in Wadi El Natrun and its districts (Fig. 1b).

The Quaternary pink deposits of sandy, thick, and pebbly sand with conglomerates cover the Pliocene deposits. The Pleistocene ruddy sand, silt, and gravels are on a very basic level scattered west of Rosetta branch and north and east of Wadi El Natrun. Windblown sand sheets and longitudinal slopes (NNW–SSE) are found in the swamp scopes of Wadi El Natrun and in the Wadi El Farigh lowlands. Lagoonal deposits are created from the trademark pools of Wadi El Natrun. Deltaic gravels and sands in the eastern part of Wadi El Natrun gradually decrease in thickness from 300 m at Rosetta branch to few meters thickness north of Wadi El Natrun [55]. The Pleistocene aquifer is the main aquifer that covers the range between the Rosetta branch and the eastern part of Wadi El Natrun. This aquifer is mostly unconfined but under semi-confined conditions at northern El Nubaria canal. The hydraulic conductivity of the Quaternary aquifer in the examined region ranges from 30 up to 77 m/day [56–58]. As indicated by Osman [59], most of the Pleistocene deposits in the investigation region are of river depositional environment with multidirectional sedimentation environment. These deposits are poorly sorted, and the mean grain estimate ranges from medium pebbles to medium sand with average size that of extremely coarse sand. The Holocene aquifer is made out of present-day sand gatherings of aeolian sandy stores with calcareous intercalations from 4 m to around 10 m thickness. It is situated in the lowland regions of Wadi El Natrun (Fig. 1b).

The surface geology of the area (Fig. 2) shows that, in the south, there are stabilized dunes and sand sheets, while Wadi deposits (sand and gravels) cover the central part around Nubaria canal. In the northern part, the surface is covered by

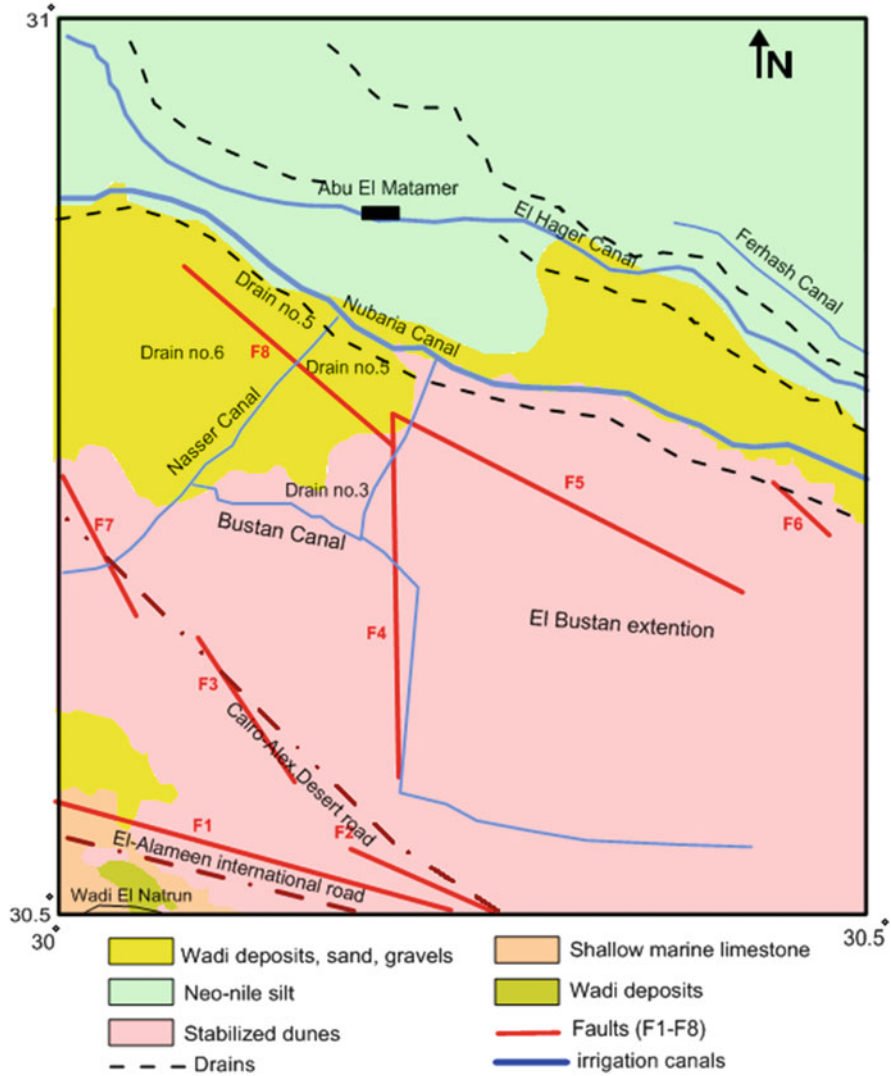


Fig. 2 Geomorphologic and structural map of the study area

neo-Nile silt and clay. The structural map of the area compiled by different authors is shown in Fig. 2. Major faults with downthrown sides due east have been delineated along the western margin of the Nile Delta. These faults have led, among other geologic features, to the facing of the highly permeable Pleistocene gravel of the Nile Delta opposite to older impermeable sediments to the west. This situation accelerates the subsurface westward flow of Nile water to the older sediments [60]. Two subsurface faults in the area were detected by El Ghazawi [61] comprising El Galala fault (F7) with downthrown to east and displacement

reaches about 65 m and El Nubaria fault (F8) with downthrown also to east (Fig. 2). They are related to tectonic system during Neogene times. However, the rapid vertical and lateral facies changes of the Quaternary sediments hide this displacement. On the other hand, four probably subsurface faults (F3, F4, F5, and F6) have been detected with downthrown to the Nile Delta [62]. They greatly affect the thickness of the Pleistocene aquifer.

Wadi El Natrun anticlinal structure trends E 35° W and extends for about 60 km from El Ralat depression in the north to Beni Salama depression in the south [63]. It is a symmetrical structure affected by parallel and diagonal faults, among them F1 and F2 that led to the formation of the central main depression (Fig. 2). Unconformities are recognized in the area between the Quaternary deposits and Pliocene deposits, where Wadi El Natrun Formation (early Pliocene) is covered directly by Quaternary clastics, and El Hagif Formation is absent (late Pliocene) [61].

Saad [64] stated that the groundwater flow direction in this area is from NE to SW and the transmissivity of the Pleistocene aquifer is 0.615–0.897 m²/min. The water level all over the area was increased by about 2.5–3 m from March 1972 to March 1973. Before reclamation projects, the groundwater seeps from El Nubaria canal to the west, but after constructing the pumping stations, the groundwater flows toward El Nubaria canal, where it acts as a drain (The Desert Institute in its internal report [65]). Abdel Baki [66] stated that the recharge in the area is from two sources: the groundwater inflow and the infiltrated water from irrigation and the groundwater depth vary widely from a few meters close to the Delta to about 60 m near the Cairo-Alexandria desert road. Recently, groundwater flow system during 2010 was constructed by Salem and Osman [19, 53]. It was found that the water table height differs from –2 m in the northern sites to more than +27 m above sea level in the southwestern direction (Fig. 3). The general groundwater flow is from south to northern and northeastern directions. The main recharge area is seen in the southern part of the territory. The groundwater likewise streams toward Wadi El Natrun in the southwestern parts. They also stated that the piezometric level difference between 1966 and 2010 revealed an increase of the water table reaching up to 30 m in the southwestern part of the area which might have occurred due to irrigation processes and seepage from the canal systems.

3 Methodology

The two basic electrical properties of the rocks are electrical resistivity and polarization. The polarization refers to a substance that exhibits a charge separation in an electric current. The resistivity of rock depends on many factors, including rock type, the conductivity of pores and nature of the fluid, and metallic content of the solid matrix. The rock resistivity is roughly equal to the resistivity of the pore fluids divided by the fraction porosity [67]. The resistivities of the common rocks and minerals are shown in Fig. 4. This work was done in three steps: data acquisition (field work), data processing, and data interpretation.

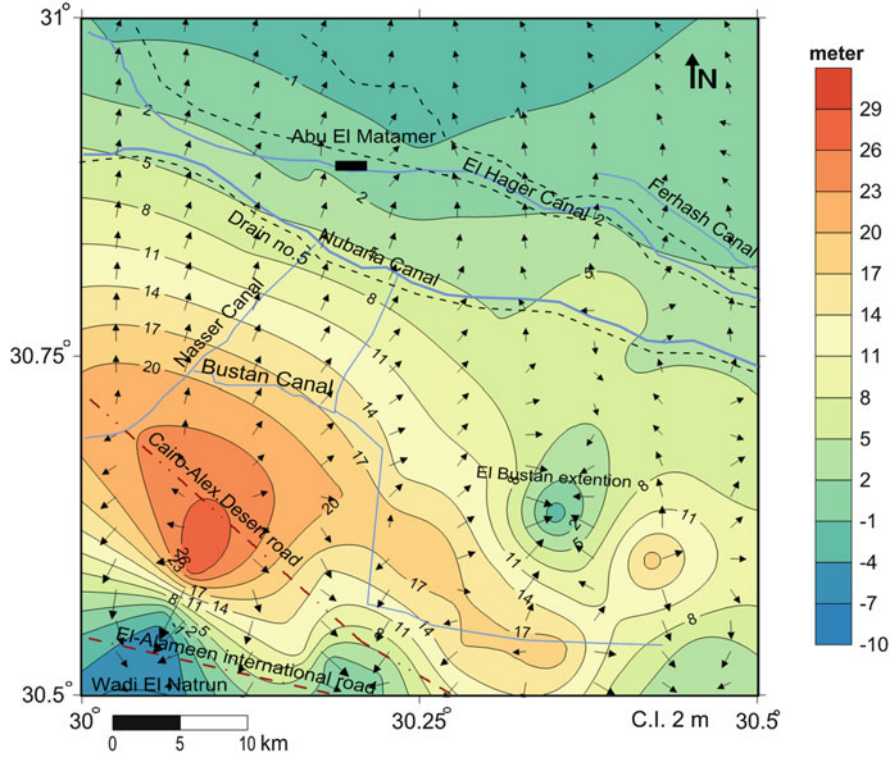


Fig. 3 Groundwater flow system in the study area (after [19])

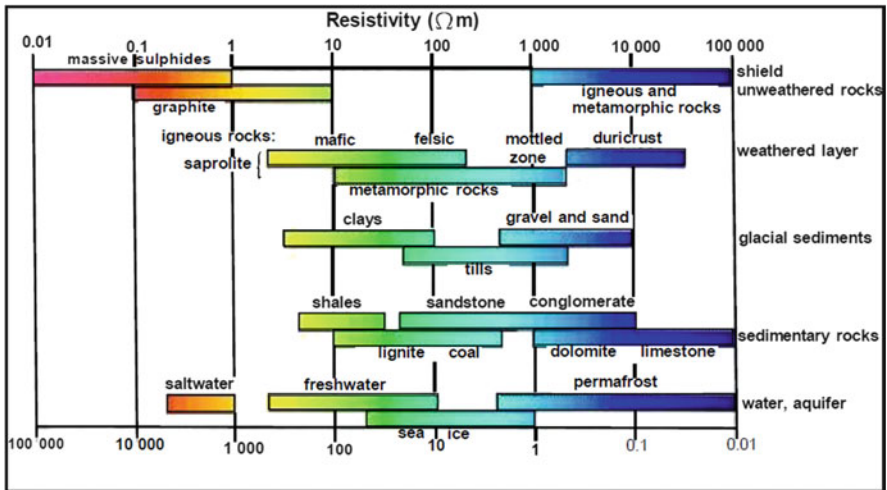


Fig. 4 Electrical properties of the common rocks and minerals [68]

3.1 Data Acquisition (Field Work)

The geoelectric survey of this work is executed by ELERIC-T SYSCAL-R2 (Fig. 5). In this work, the electrical resistivity survey was carried out in the form of vertical electrical sounding (VES), using Schlumberger 4-electrode array. Thirty-two vertical electrical soundings were measured in the study area. The VES locations were planned on topographic map for the study area (scale 1:50,000) and projected in the field by GPS instrument. The sounding points and geoelectrical cross sections were distributed to cover the area (Fig. 6). Some VES stations were located beside wells or boreholes to correlate the measured resistivity data with known geologic and lithologic successions. The current electrode spreading ($AB/2$) starts with 1–1,000 m, while the potential electrode spreading ($MN/2$) starts with 0.25–25 m to obtain a measurable potential difference. This electrode separation is sufficient to reach the required depth that fulfills the main aim of the study given the geologic and hydrogeologic information.

3.2 Data Processing

The SYSCAL R2 computes and displays the apparent resistivity automatically for the most common electrode arrays (Schlumberger and Wenner sounding and profiling, gradient, dipole-dipole, etc.) in the field, i.e., it has automatic processing software. Data interpretation can be made qualitatively and quantitatively. The qualitative interpretation gives initial information about layer numbers, resistivity, direction, and homogeneity degree. The quantitative interpretation determines



Fig. 5 The used Earth resistivity instruments (ELERIC-T, SYSCAL R2)

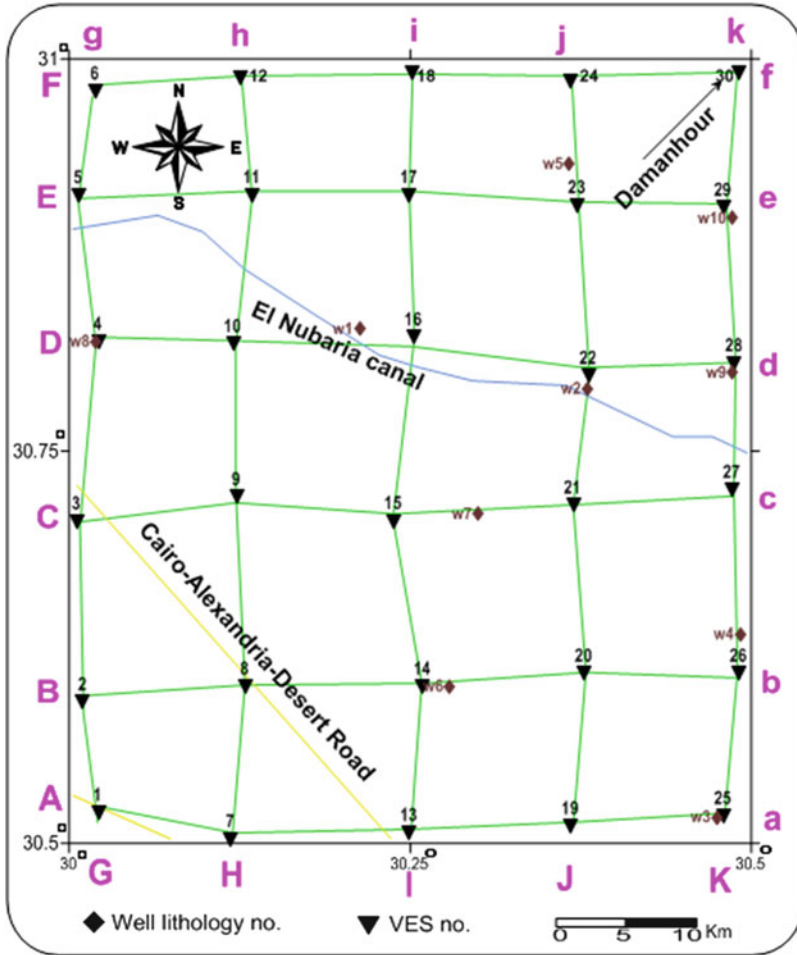


Fig. 6 Location map of the soundings (VESs) and geoelectrical cross-section distribution in the area

geoelectrical layers, true depth, thickness, and resistivity of each layer. The geophysical boundaries may cross over different lithologies and may not coincide with lithologic boundaries or geologic formation boundaries.

3.3 Data Interpretation

There are many computer programs commonly used in quantitative interpretation. In this work, a program called IPI2win, version 2.0 [69], was used. The obtained lithology (thickness, type) data from the nearby wells was used as a preliminary 1D

model for regularizing the process of the fitting error minimization. An important advantage of this program is the concept of interpreting a profile, where its points are treated as a unity representing the geological structure of the survey area as a whole, rather than a set of independent objects dealt with separately.

According to geologic information and nearby wells lithology to the VES stations, a good starting model for each one is used during the inverse modeling operation by using IPI2win software. The fixing option in this program is used to fix some parameters of the model to not be free during the inverse modeling process. By this way, all the available layer thickness which obtained from some wells are introduced as a ground truth. Also, reliable geoelectric cross sections are constructed by reinterpretation of some VES according to the results obtained from interpretation of the neighbored ones. The final model which is calculated by using this program is given in the appendix. Also, the interpreted layer parameters in the form of true resistivities and thicknesses of the surface geoelectric layers of these soundings are listed in Table 1. The aquifer depth, aquifer thickness, and water table are shown in Table 2.

4 Results and Discussion

4.1 Resistivity Spectrum

There are many VESs carried out beside drilled wells in the area to calibrate its resistivity results with those of well lithology. These calibrations reveal a good matching of the interpreted resistivities with the lithology layers (Fig. 7) and give a good resistivity spectrum for the area. The electric resistivity of sediments depends on lithology, clay and water contents, as well as salinity [21]. Therefore, the resistivity spectrum shows a wide range of resistivity values. So, there is an importance to correlate the wells lithology with the VES values to ensure the final results. The resistivity spectrum of this work is shown in Table 3.

4.2 Geoelectrical Cross Sections

There are 11 cross sections at different locations and directions; they are constructed from the deduced layer parameters. These include six lateral cross sections in an east-west direction containing five VES points and five traverse cross sections in a north-south direction having six VES points. The main purpose of these cross sections is clarifying two-dimensional pictures for the subsurface layer distributions (depth, thickness, lithology, aquifer extension, and seawater intrusion limitation). These cross sections mainly consist of four layers. They are surface, sand (fine sand with intercalations of clay, medium to coarse sand), clay layers (clay and sandy clay), and brackish water to saltwater.

Table 1 The obtained true resistivities and thicknesses of the detected geoelectric layers

No.	Lat. (N)	Long. (E)	Elev. (m)	Layer 1		Layer 2		Layer 3		Layer 4		Layer 5		Layer 6	
				ρ (Ω)	h (m)	ρ (Ω)	h (m)	ρ (Ω)	h (m)	ρ (Ω)	h (m)	ρ (Ω)	h (m)	ρ (Ω)	h (m)
1	30.52	30.02	30	17	8	6	23	21	60	15					
2	30.58	30.01	37	10	4	2	10	5	25	15	80	2.6			
3	30.71	30.00	30	9.3	1.5	68	1.5	15	60	5					
4	30.82	30.02	19	10	3	15	29	5	45	2.5					
5	30.92	30.00	0	8	1.5	6	19	10	22	2.5					
6	30.98	30.02	-3	15	1.5	5	17	2.5	25	1					
7	30.50	30.12	40	30.2	1	7.2	10	15.8	13	6.2	25.3	15			
8	30.57	30.13	31	77.4	3	24	15	5							
9	30.72	30.12	25	131	1.3	66.8	1.3	25.9	18.4	15.3	59	5	37.5	1	
10	30.82	30.12	12	22.4	1.5	65	2	17	25	34	36	8			
11	30.92	30.13	-3	33.2	1	5	58	1							
12	30.99	30.13	-3	10	0.5	6	15	2.5	22	1					
13	30.51	30.25	36	17	9	28.2	100	5							
14	30.60	30.27	28	510	4	12	7	8	40	24	60	3			
15	30.71	30.24	21	109.5	3.3	20.4	90	5							
16	30.83	30.25	6	12.3	1	35	6	18	30	46	38	5.4			
17	30.92	30.25	-2	16	3.5	7	16	15	28	6	36	1			
18	31.00	30.25	-2.5	10.6	2	6	15	2.7	22	1					
19	30.52	30.40	30	37	1	23	4	307	8	21	86	4			
20	30.61	30.37	27	31.5	1	18.2	5	184	4.3	8	40	24			
21	30.72	30.37	18	73.6	1	261	1.3	10	4	26	120	8			
22	30.80	30.38	6	70.8	1.5	5.9	1	17	45	30	55	14			
23	30.91	30.38	-2	16	1.5	12	9.5	23	35	8	42	1.4			
24	30.99	30.37	-4	4.2	0.5	27.7	0.5	11	32	6	35	1			

25	30.52	30.48	32	163	1.9	25	2.5	296	17	26	47	23
26	30.61	30.50	21	91	2	116	9	50	54.7	29		
27	30.73	30.49	10	55	4	7.9	50	24.6	65	7.2		
28	30.81	30.49	4	39.6	2.9	9.1	2.1	20.1	13	14.2	13.4	61.2
29	30.91	30.48	3	10.1	1.5	142	3.3	16	31	44	44.3	7.2
30	31.00	30.50	3	7.2	2	2.5	7	59.5	67	6.6		

Table 2 The hydrogeological parameters of the Pleistocene aquifer of the study area

No.	Water level	Water table	Aquifer depth	Brackish water depth	Aquifer thickness	Aquifer resistivity	Average surface resistivity
1	-24	6	24			18	17
2	-31.9	5.1	31.9			15	6
3	-2.8	27.2	2.8			15	40
4	-1.9	17.1	1.9			15	10
5	-1.5	-1.5	1.5				8
6	0.5	-2.5	0.5	44	44		15
7	-13.4	26.6	13.4			15	23
8	-21	10	21				50
9	-2.5	22.5	2.5	117	114.5	21	100
10	-1.7	10.3	1.7			26	43
11	-0.4	-3.4	0.4	60	59.6		33
12	-0.3	-3.3	0.3	38	37.7		10
13	-13	23	13			28	17
14	-6.7	21.3	6.7			24	260
15	-3.3	17.7	3.3			20	110
16	-1	5	1			32	25
17	-0.5	-2.5	0.5	84	83.5	15	16
18	-1	-3.5	1	40	39		10
19	-19.5	10.5	19.5			21	122
20	-24.1	2.9	24.1			24	228
21	-12	6	12			26	115
22	-1.6	4.4	1.6			24	26
23	-1.2	-3.2	1.2	88	87	23	16
24	-1	-5	1	58	57		28
25	-21.7	10.3	21.7			25	160
26	-14.5	6.5	14.5			40	70
27	-4	6	4			25	55
28	-4.9	-0.9	4.9			52	25
29	-2.7	0.3	2.7			30	76
30	-1.2	1.8	1.2			60	7

4.2.1 Cross-Section Aa

This cross section passes at the southern part of the area from east to west and includes five VES stations (1, 7, 13, 19, and 25). The geoelectric horizons (Fig. 8) are (from top to bottom):

1. The surface layer: its resistivity ranges from 16 (VES no.7) to 307 Ω m (VES no.19). It consists of sand, calcareous sand, and shale. Its thickness varies from 10 to 25 m.

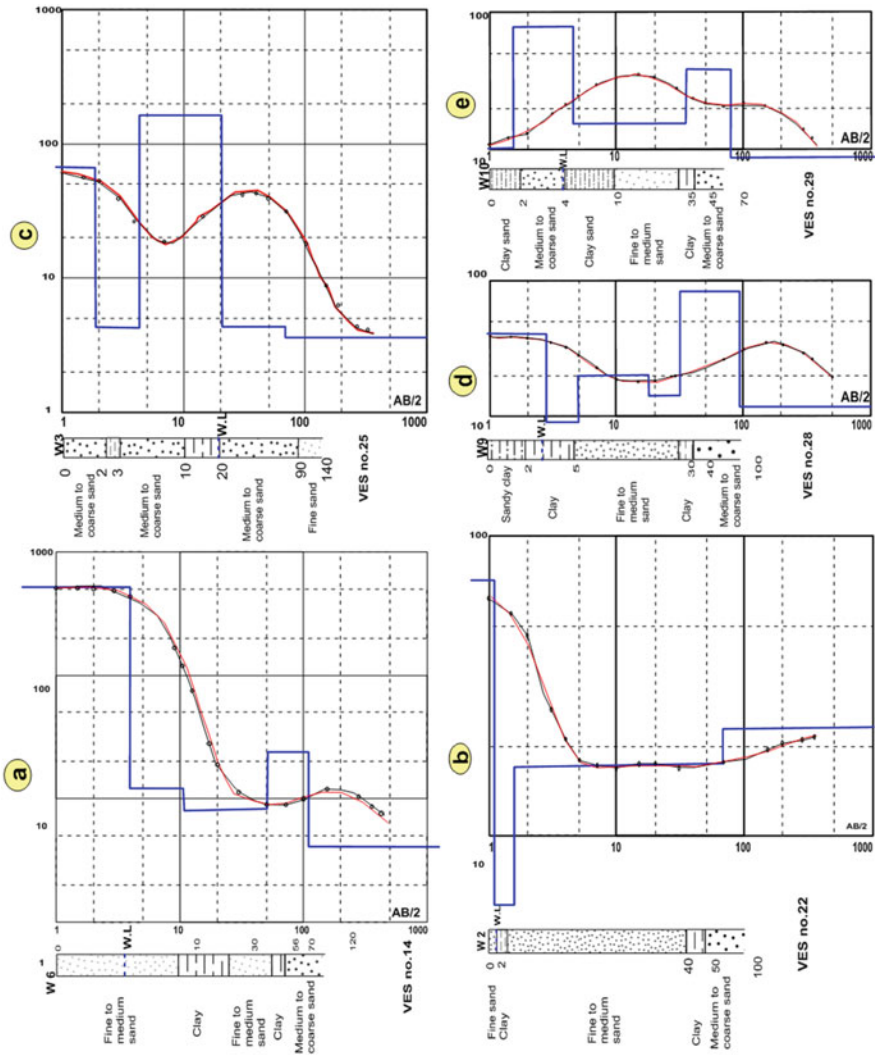


Fig. 7 Examples of the calibration between interpreted VES and lithology of the nearest wells of the study area (a, VES 14; b, VES 22; c, VES 25; d, VES 28; and e, VES 29)

Table 3 Resistivity spectrum results of the detected layers in the study area

No.	Phase	Lithology type	(Ω m)
1	Surface layers (dry)	Sand, clay, gravels, . . . etc.	10–500
2, 3	Saturated zone	Medium to coarse sand	30–90
		Clayey sand	15–30
		Sandy clay	5–15
		Clay	2–10
4	Brackish water to saltwater zone		<2

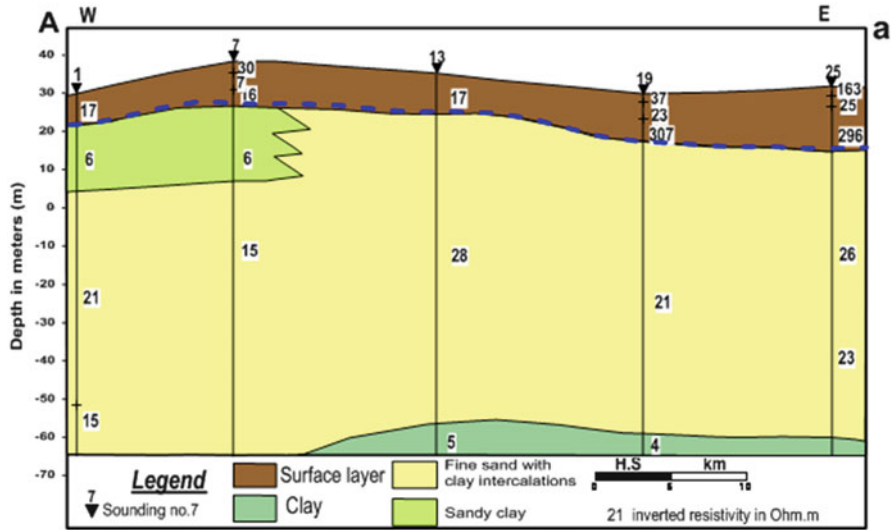


Fig. 8 Geoelectric cross section along profile Aa (W-E) in the study area

2. Aquifer layers: resistivity ranges from 15 to 28 Ω m and it consists of fine sand with intercalations of clay. The thickness varies from 60 m (VES no. 19) to 90 m (VES no. 13).
3. Clay layers: resistivity varies from 4 to 6 Ω m (VES no.19, 7, respectively). They are composed of clay at the base of VES no. 13, 19 and 25 and sandy clay between the surface and fine sand in VES no. 1 and 7.

4.2.2 Cross-Section Bb

It also extends from east to west and lies in the southern part of the area (Fig. 9). This cross section contains five VESs (2, 8, 14, 20, and 26). Interpretation of cross-

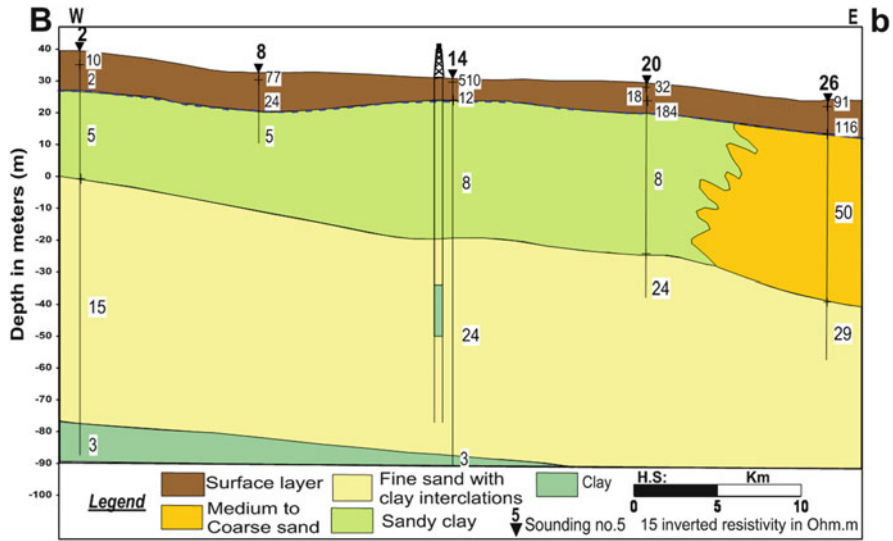


Fig. 9 Geoelectric cross section along profile Bb (W-E) in the study area

section VESs is mainly constrained by the geologic information from the drilled well close to sounding no. 14; the layers of this section are:

1. The surface layer: its resistivity ranges from 10 to 512 Ω m (VES 2 and 14) with a variable thickness ranging from 10 to 18 m (VES 20 and 8).
2. Aquifer layers: resistivity ranges from 15 to 50 Ω m (VES 2 and 26), and the thickness varies from 60 m to unknown value (VES 14 and 26). These layers are composed of fine sand with clay intercalations and medium to coarse sand.
3. Clay layers: their resistivities vary from 3 to 8 Ω m (VES no. 2 and 4). They are composed of clay at the base (VES no. 2 and 14, 20) and sandy clay between surface and fine sand (VES no. 2 and 20) with thickness ranging between 25 m and 40 m (VES no. 2 and 20).

4.2.3 Cross-Section Cc

The geoelectric cross section along this profile contains five soundings; they are 3, 9, 15, 21, and 27 (Fig. 10). This section lies at the southern central part of the area. It extends from west to east and consists of the following geoelectric horizons:

1. The surface layer: Its resistivity ranges from 10 to 261 Ω m (VES 3 and 21), while the thickness varies from 2.6 to 6.3 m (VES 9 and 21).
2. The aquifer layers: With resistivity ranging from 15 to 26 Ω m (VES 3 and 21). The thickness ranged from 60 to 120 m (VES 3 and 21) and is composed of fine sand with clay intercalations.

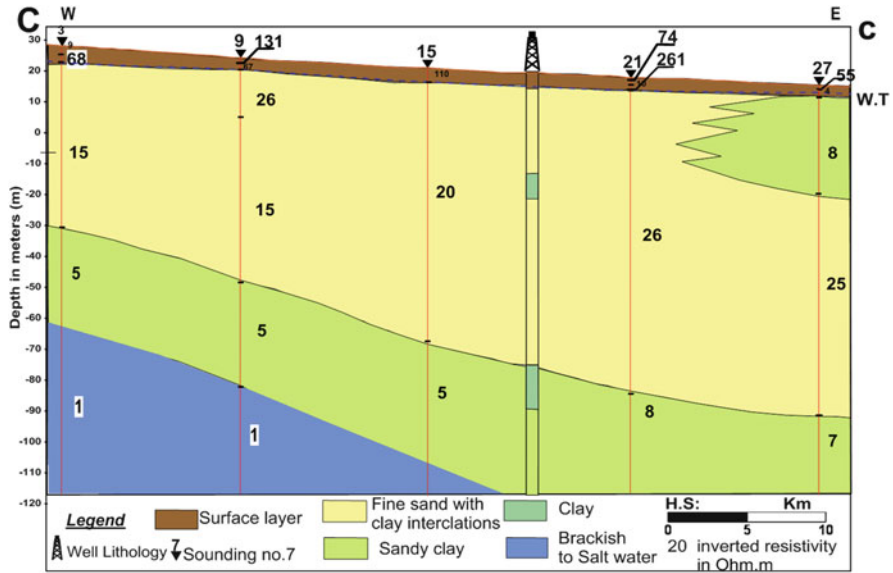


Fig. 10 Geoelectric cross section along profile Cc (W-E) in the study area

3. The clay layer: Its resistivity ranges from 5 to 9.3 Ω m (VES 3, 9, 15 to 21, 27). The thickness varies from 37.5 m (VES 9) to unknown value at the rest of the cross section.
4. The brackish water to saltwater intrusion zone: Its resistivity in the range of 1 Ω m and depth - 90 m (VES 9) and to be expected in VES no. 3 and 15 (Fig. 10).

4.2.4 Cross-Section Dd

This cross section is parallel to the previous cross section and lies in the north-central part extending from west to east. It contains five soundings; they are 4, 10, 16, 22, and 29. It includes the following geoelectric layers (Fig. 11):

1. The surface layer: its resistivity ranges from 6 to 71 Ω m (VES no. 22), and thickness varies from 2.5 to 7 m (VES 22 and 16).
2. The aquifer layers: can be differentiated into two zones:
 - (a) Fine sand with clay intercalations: at the top with resistivity ranging from 15 to 20 Ω m (VES 4 and 28). The thickness varies from 25 to 30 m (VES 10 and 16).
 - (b) Medium to coarse sand: at the base with resistivity ranging from 30 to 83 Ω m (VES no. 22 and 28). Its thickness varies from 36 to 61 m (VES no. 10 and 28).

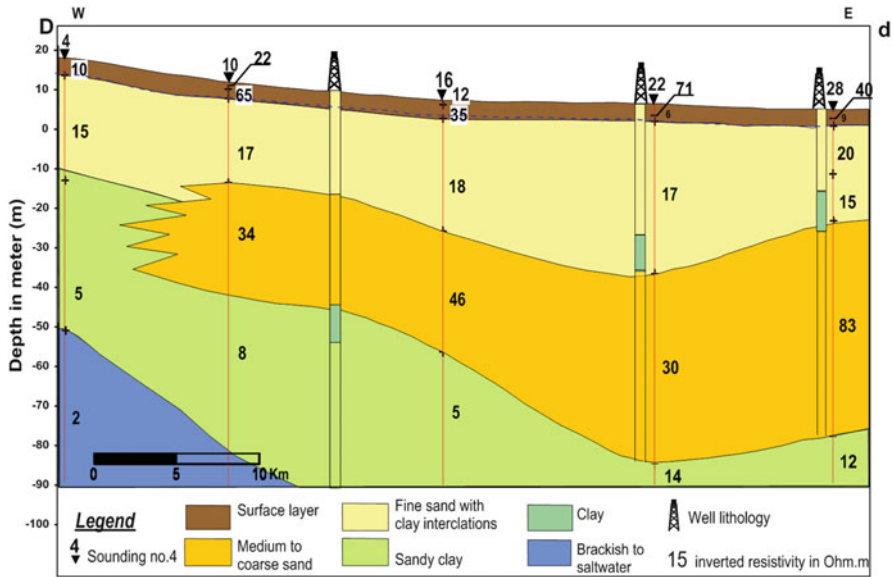


Fig. 11 Geoelectric cross section along profile Dd (W-E) in the study area

3. The clay layer: with resistivity ranging from 2 to 14 Ωm (VES 4 and 22), and thickness varies from 45 m (VES 4) to unknown value in the others. It is composed of sandy clay and clay.

4.2.5 Cross-Section Ee

This cross section includes five VES stations (5, 11, 17, 23, and 29). It extends from the west to the east and lies to the north and parallel to the previous cross sections. This cross section (Fig. 12) consists of the following layers:

1. The surface layer: with resistivity ranging from 8 to 142 Ωm (VES 5 and 29) and thickness from 1 to 3.5 m (VES 11 and 17).
2. The aquifer layers: the resistivity ranges from 15 to 44 Ωm (VES 17 and 29). The thickness varied from 30 to 75 m (VES 15 and 29) and is composed of fine sand with clay intercalations and medium to coarse sand.
3. The clay layer: its resistivity ranges from 5 to 12 Ωm (VES 11 and 23). The thickness varies from 52 to 69 m (VES 5 and 11).
4. The brackish water to saltwater intrusion zone: the resistivity is less than 2 Ωm (VES 5, 11, 17, 23). Its depth ranges from -47 to -100 m (VES 5 and 23).

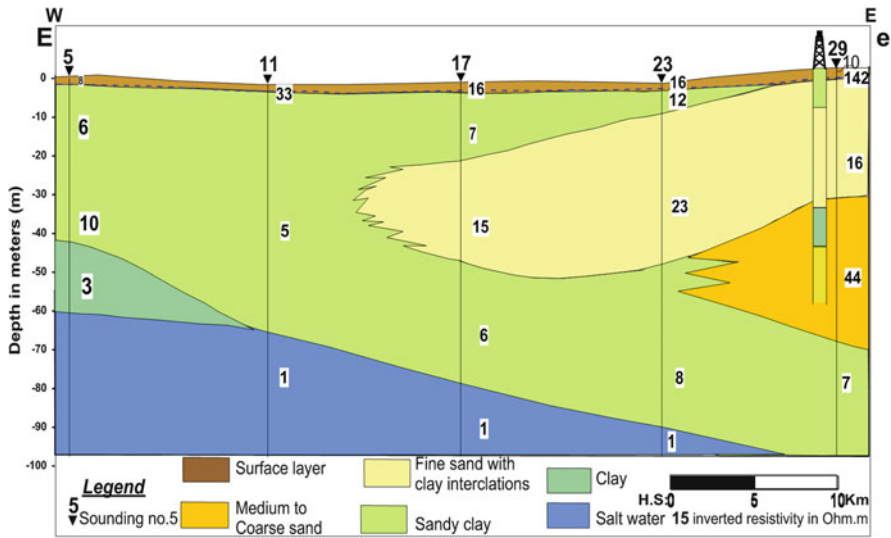


Fig. 12 Geoelectric cross section along profile Ee (W-E) in the study area

4.2.6 Cross-Section Ff

This cross section lies in the most northern part of the area and extends from west to east direction parallel to the previous cross sections. It includes five VES stations (6, 12, 18, 24, and 30). The sedimentary succession is (Fig. 13) as follows:

1. The surface layer: Its resistivity ranges from 6 to 28 Ω m (VES 12 and 24). The thickness varies from 1 to 2.5 m (VES 12 and 30).
2. The aquifer layers: Resistivity is 60 Ω m and thickness is 67 m (VES 30). They are composed of medium to coarse sand.
3. The clay layer: Its resistivity is 2 Ω m (VES 6, 12, 18), and the thickness varies from 30 to 35 m (VES 6, 12).
4. The brackish water to saltwater intrusion zone: Its resistivity is less than 2 Ω m (all cross-section VES). The depth ranges from -35 to -57 m (VES 6, 18).

4.2.7 Cross-Section Gg

This cross section lies in the western part of the area and extends in NS direction. It includes six VES stations; they are 1, 2, 3, 4, 5, and 6. The geoelectric layers (Fig. 14) are the following:

1. The surface layer: Its resistivity ranges from 2 to 68 Ω m (VES 2 and 3), and thickness from 2 to 14 m (VES 6 and 2).

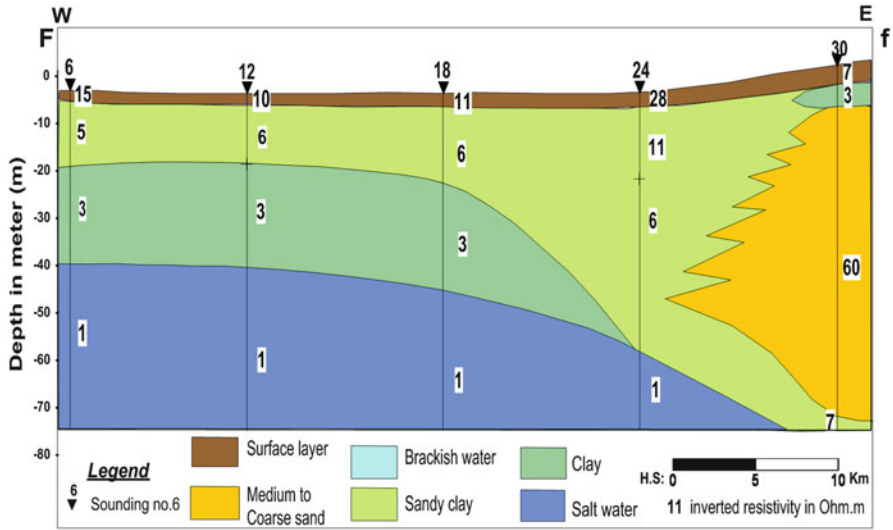


Fig. 13 Geoelectric cross section along profile Ff (W-E) in the study area

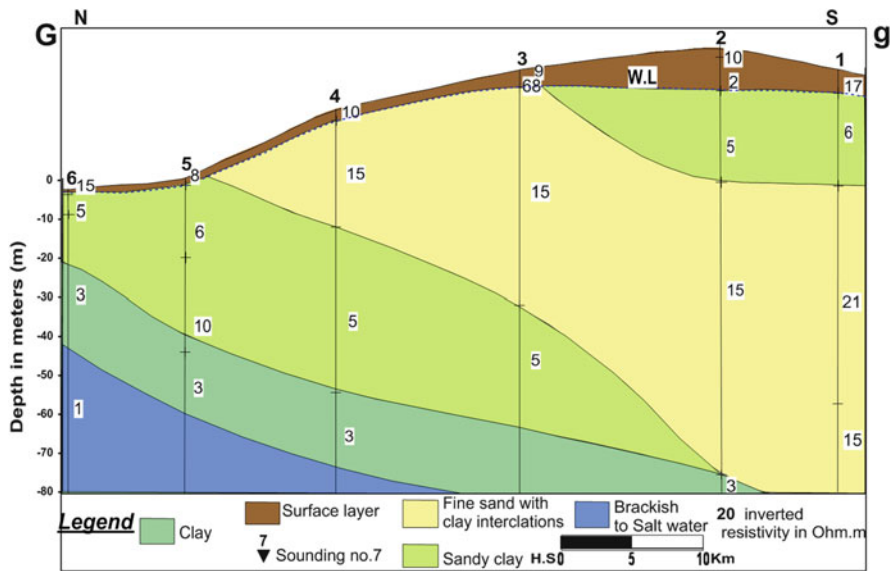


Fig. 14 Geoelectric cross section along profile Gg (N-S) in the study area

2. The aquifer layers: The resistivity ranges from 15 to 21 Ω m (VES 1, 2, 3, 4, and 1) and the thickness from 29 to 80 m (VES 4 and 2). The aquifer is composed of fine sand with clay intercalations.
3. The clay layer: Its resistivity ranges from 5 to 10 Ω m (VES 2, 3, 4, and 5) and thickness from 23 to 52 m (VES 1 and 5). It is composed of sandy clay and clay layers (at the base of the cross section).
4. The brackish water to saltwater intrusion zone: Its resistivity is less than 2 Ω m, and depth is -37 m (VES 1).

4.2.8 Cross-Section Hh

This cross section lies in the central western part of the area and extends in NS direction. It includes six VES stations; they are 7, 8, 9, 10, 11, and 12 and extend parallel to the previous one. The geoelectric layers (Fig. 15) are the following:

1. The surface layer: Its resistivity value ranges from 10 to 131 Ω m (VES 12 and 9), and the thickness ranges from 1 to 18 m (VES 12 and 8).
2. The aquifer layers: Resistivity ranges from 15 to 34 Ω m (VES 9 and 10), and the thickness varies from 61 to 77 m (VES 10 and 9). They are composed of fine sand with clay intercalations and medium to coarse sand.

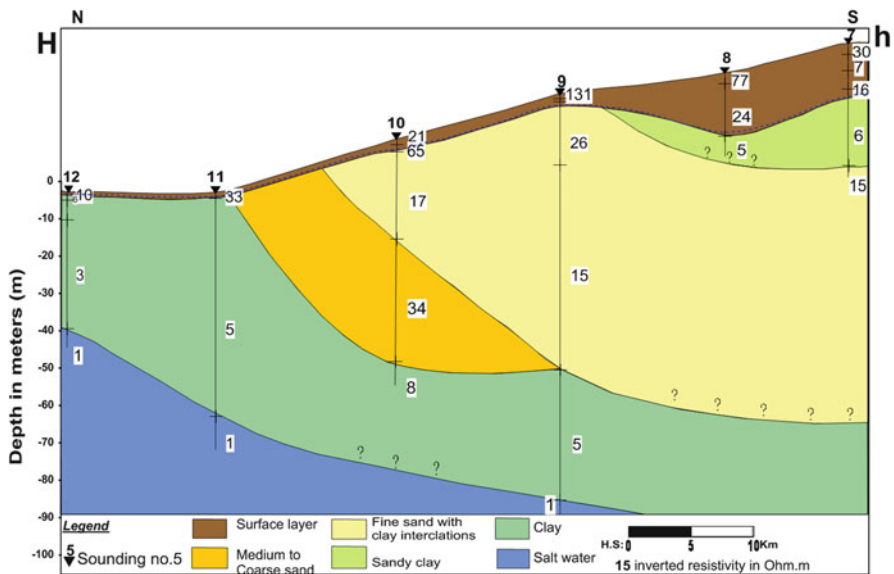


Fig. 15 Geoelectric cross section along profile Hh (N-S) in the study area

3. The clay layer: Its resistivity ranges from 2 to 8 Ω m (VES 12 and 10), and the thickness varies from 25 to 69 m (VES 7 and 11). It is composed of sandy clay layers at the top and clay layers at the base of the section.
4. The brackish water to the saltwater zone: Its resistivity is less than 2 Ω m (VES 9, 11, 12), and the depth varies from -37 to -90 m b.s.l (VES 12 and 9).

4.2.9 Cross-Section II

This cross section lies in the middle part of the area and extends in NS direction. It includes six stations; they are 13, 14, 15, 16, 17, and 18. The geoelectric layers of this section (Fig. 16) are the following:

1. The surface layer: Its resistivity ranges from 10 to 510 Ω m (VES 18 and 14), and the thickness varies from 2 to 14 m (VES 18 and 14).
2. The aquifer layers: The resistivity ranges from 15 to 46 Ω m (VES 17, 16), while the thickness varies from 30 to 90 m (VES 17 and 16). They are composed of fine sand with clay intercalations and medium to coarse sand (VES 16).
3. The clay layers: With resistivity ranges from 2 to 8 Ω m (VES 14 and 18) and thickness from 8 to 40 m (VES 18 and 14). They are composed of sandy clay and clay layers (base of the section).
4. The brackish water to saltwater intrusion zone: Its resistivity is less than 2 Ω m (VES 17 and 18).

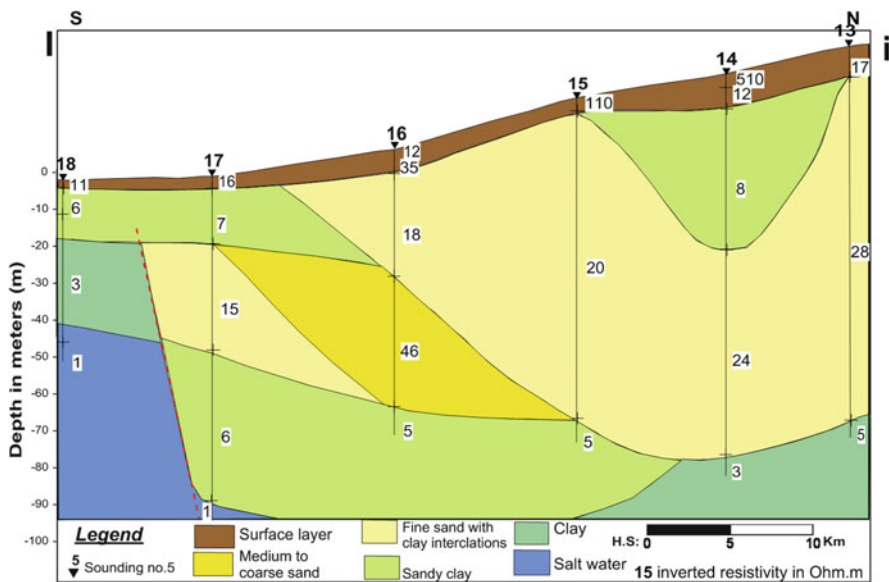


Fig. 16 Geoelectric cross section along profile Ii (S-N) in the study area

4.2.10 Cross-Section Jj

This cross section lies in the central eastern part of the area and extends in NS direction. It includes six VES stations; they are 19, 20, 21, 22, 23, and 24. The geoelectric layers of this section (Fig. 17) are the following:

1. The surface layer: Its resistivity ranges from 6 to 307 Ω m (VES 22 and 19), and the thickness ranges from 1 to 13 m (VES 24 and 19).
2. The aquifer layers: The resistivity ranges from 17 to 30 Ω m (VES 22). Its thickness ranges from 40 to 120 m (VES 23 and 21). They are composed of fine sand with clay intercalations and medium to coarse sand.
3. The clay layer: Its resistivity ranges from 4 to 14 Ω m (VES 19 and 22). The thickness of this layer ranged from 35 to 40 m (VES 24 and 20) and is composed of sandy clay and clay beds.
4. The brackish water to saltwater intrusion zone: Its resistivity is less than 2 Ω m (VES 23, 24).

4.2.11 Cross-Section Kk

This cross section lies in the eastern part of the area and extends in NS direction. It includes six VES stations; they are 25, 26, 27, 28, 29, and 30. The geoelectric layers of this section (Fig. 18) are the following:

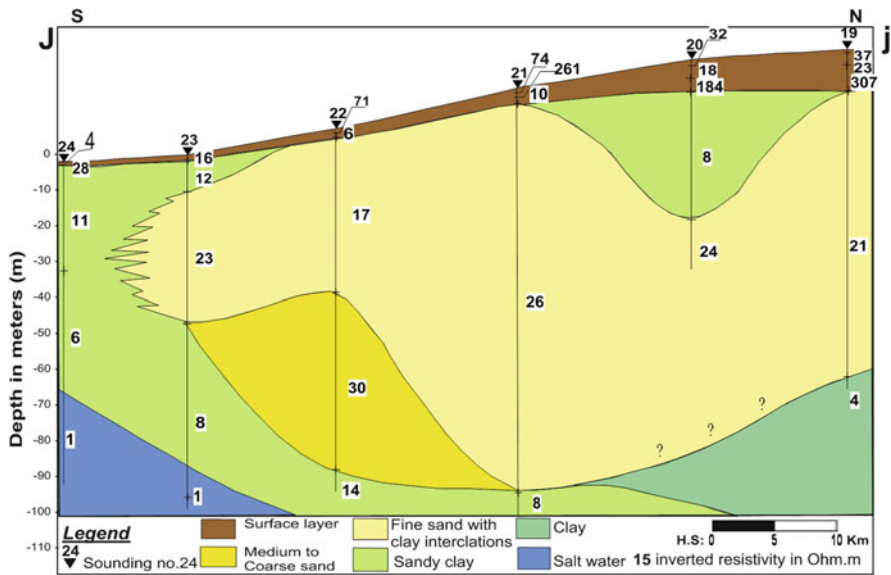


Fig. 17 Geoelectric cross section along profile Jj (S-N) in the study area

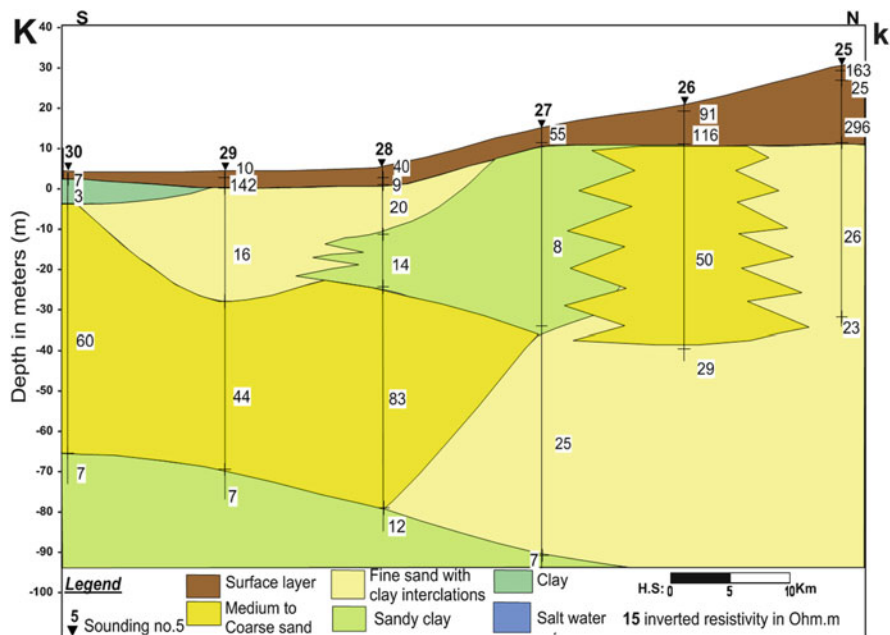


Fig. 18 Geoelectric cross section along profile Kk (S-N) in the study area

1. The surface layer: Its resistivity ranges from 7 to 296 Ω m (VES 30 and 25) with thickness varying from 2 to 21.5 m (VES 30 and 25).
2. The aquifer layers: The resistivity ranges from 16 to 83 Ω m (VES 29 and 28). The thickness varies from 65 m to unknown value (VES 27 and 25, 26). They are composed of medium to coarse sand and fine sand with clay intercalations.
3. The clay layer: Its resistivity ranges from 3 to 14 Ω m (VES 30 and 28), and the thickness varies from 2 to 50 m (VES 30 and 27). It is composed of sandy clay and clay layers.

4.3 Geoelectrical Maps

Several isoparametric maps have been constructed to illustrate the lateral variations of the geoelectrical data all over the area. The following are the description and interpretation of these maps:

4.3.1 The Surface Layer

This layer represents the recent deposits, deltaic deposits, stabilized dunes, and neo-Nile deposits. It exhibits a wide resistivity value ranging in average from 20 up

to 240 Ω m. The true resistivity geoelectric map of this upper layer (Fig. 19) shows that the maximum value (240 Ω m) is toward the southeast of the area, reflecting the low salinity of sand dunes. On the other hand, the minimum value (20 Ω m) is recorded toward the northwestern parts of the area, due to the soil type (clay materials) that characterized by high salinity value. The thickness distribution map of the surface deposits (Fig. 20) shows an average thickness ranging from less than 1 m to more than 30 m. The maximum value (30 m) is toward the southwestern parts of the area, while the minimum value (1 m) is recorded in the north and northwestern parts of the area.

4.3.2 The Aquifer Layers

These layers are water saturated and composed of medium to coarse sand, gravel, and fine sand with clay intercalation. The layers exhibit a resistivity range from

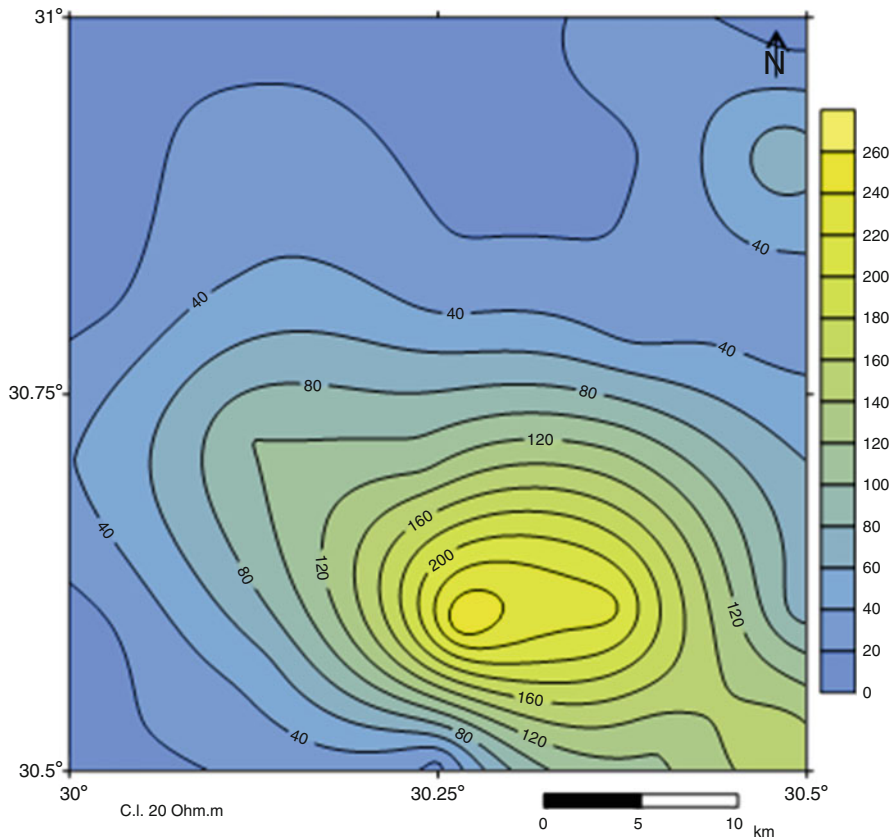


Fig. 19 The average surface layer resistivity of the area as deduced from resistivity electrical method

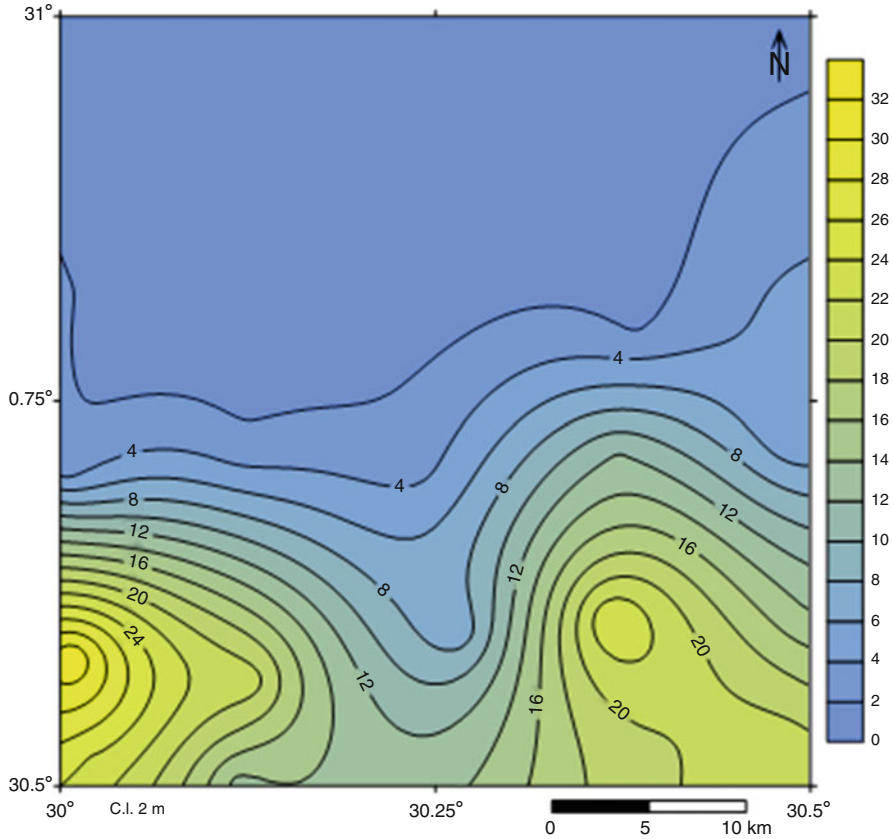


Fig. 20 The surface layer thickness of the area as deduced from resistivity electrical method

15 to 60 Ω m all over the area (Fig. 21). The minimum resistivity value is toward the northwestern parts, indicating seawater intrusion in this direction, while the maximum resistivity value is noted at the eastern parts toward the freshening water recharge from surface canals (as El Hager, Ferhash, El Nubaria). The aquifer thickness (Fig. 22) ranges from 40 up to 150 m. The minimum thickness is 40 m at the northwestern parts due to the effect of seawater intrusion. The maximum thickness (150 m) is recorded in the central part, and the aquifer thickness is increased toward the southeastern parts. It must be noted that the resistivity method applied here seldom reach more than 150 m.

4.3.3 The Seawater Intrusion Limitations

In the present study, the resistivity of the brackish water to saltwater zone is less than 2 Ω m as deduced from resistivity method. The seawater intrusion depth ranges

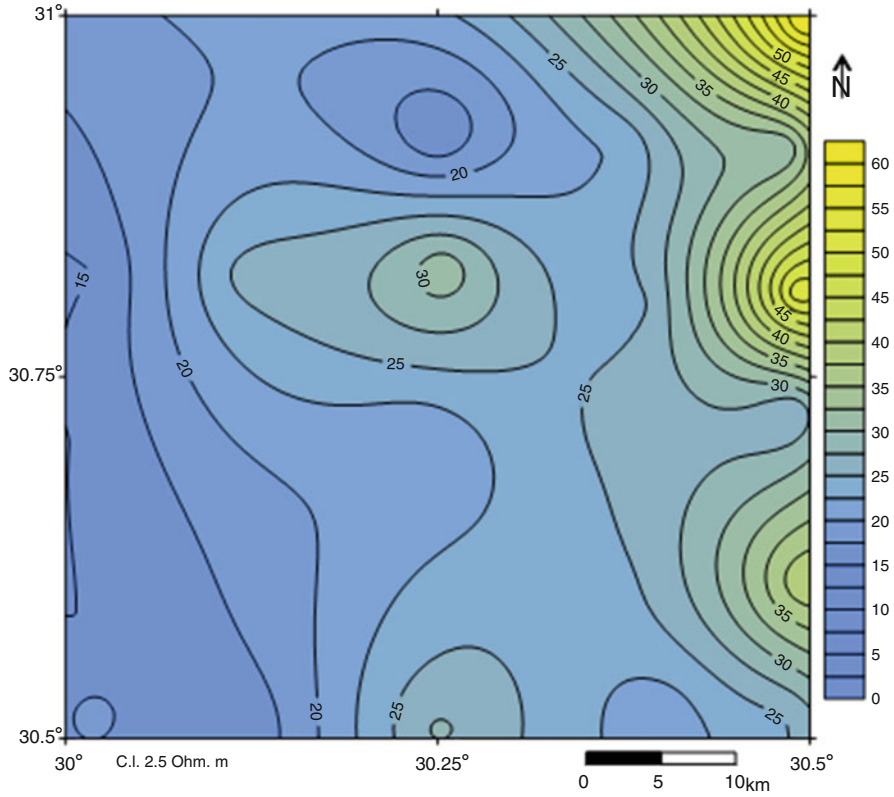


Fig. 21 The freshwater zone resistivity of the area as deduced from resistivity electrical method

from 40 to 150 m b.s.l (Fig. 23). The minimum depth reaches about 40 m in the northwestern parts of the area due to seawater intrusion. The maximum depth (150 m) is recorded toward the central parts. The applied resistivity method did not reach the seawater intrusion zone in the south and southeastern portions of the area.

4.4 3D Resistivity Model

The interpreted true resistivities and thicknesses at all sounding points are interpolated to construct the 3D model. The interpreted parameter was used to visualize the area in the form of 3D and 2D slices by using commercial Rockwork Software [70] to build solid geophysical models for the area in 3D of the dataset.

The model (Fig. 24a, b) illustrates the location of high resistivity zone in the southern and eastern directions with an average of 30–90 Ω m. Cutoff model is

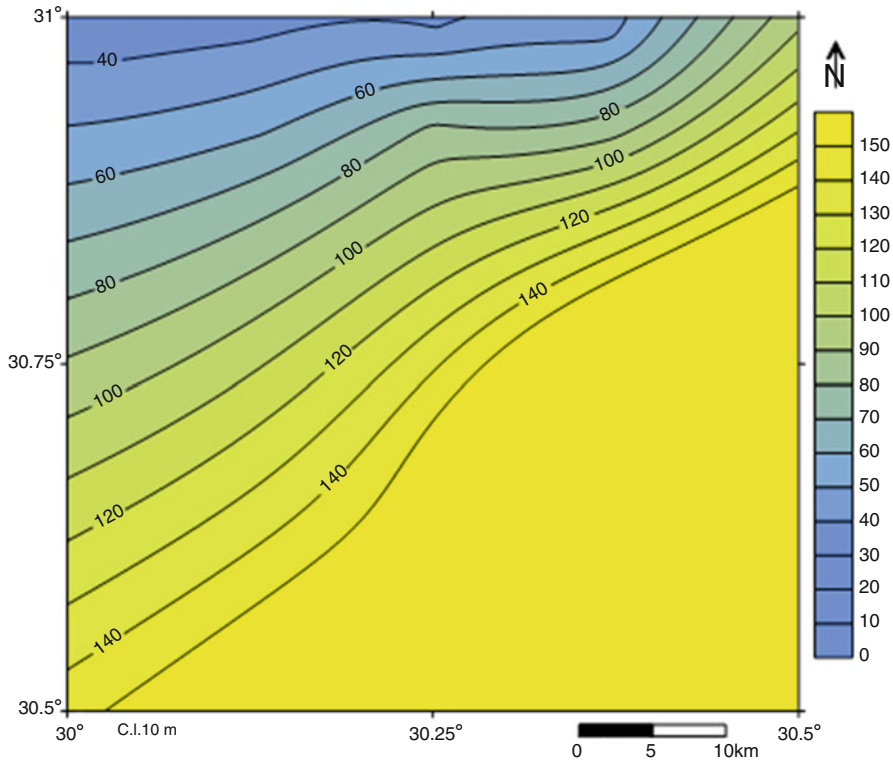


Fig. 22 The freshwater zone thickness of the area as deduced from resistivity electrical method

constructed for this resistivity zone to show only the thickness and depths of this zone which would be interpreted as the groundwater aquifer of the study area. It shows resistivity range from about 30–90 Ω at a depth range from the land surface (at the northwestern portions) and extends to nearly 30 m (at the southern portions) of the study area.

2D slices in the E-W and N-S directions of the resulted 3D model (Fig. 24c, d) were carried out to understand the lateral and vertical extension of the aquifer in the study area. It must be emphasized that the scale relations and orientations of the X, Y, and Z axes are changed for a better perspective view of the variation. The S-N slices show linear high resistivity in the south that decreases to north direction reflecting seawater intrusion trend. The east-west slices show that the main trend of high resistivity zone is toward the east direction.

The horizontal slices (Fig. 24e) reflect the high resistivity zone in the shallow depths at the southern part of the area as a result to dry surface layer. This value is decreased with depth until reaching the low resistivity zone of the brackish water. Finally, the resistivity cutoff (Fig. 24f) illustrates the aquifer of the study area in 3D direction. It shows that the great thickness is at the southeastern portions which decrease to the northwestern direction toward the seawater intrusion trend.

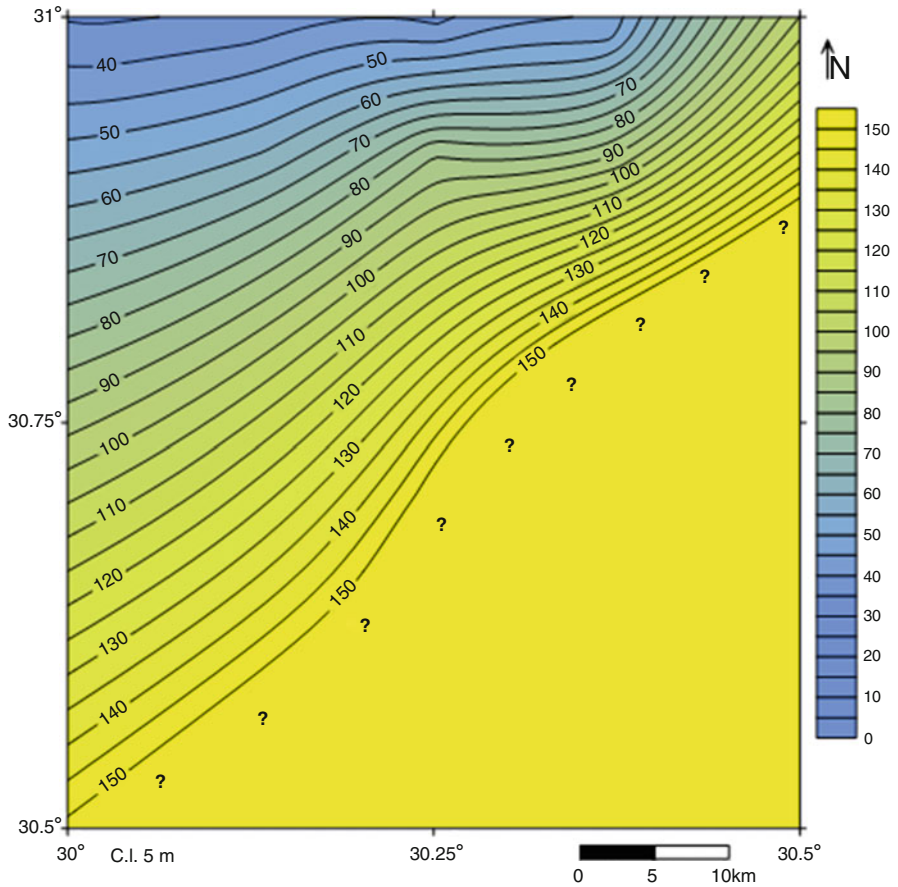


Fig. 23 The brackish water to saltwater zone depth of the area as deduced from resistivity electrical method

5 Conclusions

The resistivity data revealed four geoelectrical layers, they are:

1. The surface layer: This is composed of sand, clay, and silt. Its resistivity ranges from 5 to 512 Ω , and the thickness varies from 1 to 25 m.
2. The aquifer layer: Is composed of sand (fine sand with intercalations of clay and medium to coarse sand). Its resistivity ranges from 15 to 90 Ω m and thickness from 25 to 120 m.
3. The clay layer: Its resistivity ranges from 2 to 15 Ω m and thickness from 2 to 69 m.
4. The brackish water to saltwater intrusion zone: Its resistivity is nearly 1 Ω m, and its depth ranges from -35 in the northwest to -100 m in the south.

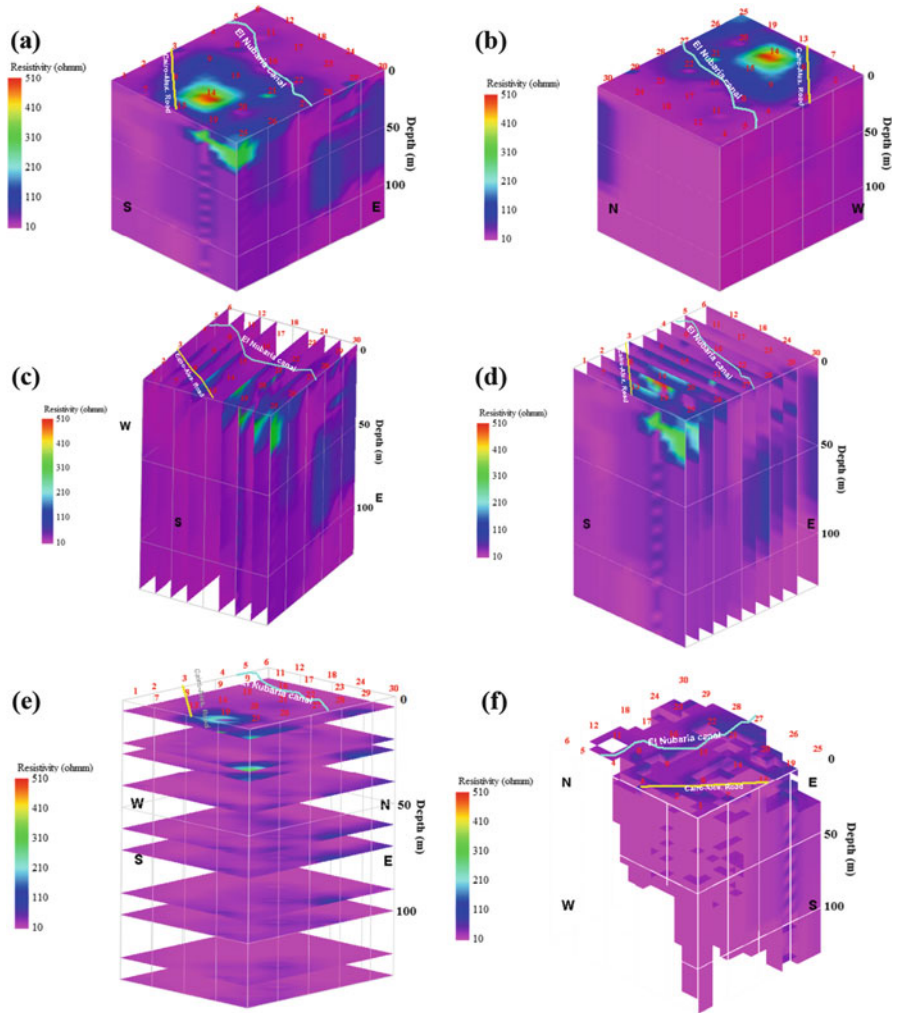


Fig. 24 3D presentation of the resistivity distribution, (a, b) resistivity solid diagram, (c) west-east slices, (d) south-north slices, (e) horizontal slices, and (f) resistivity cutoff diagram

The resistivity of the aquifer layer is increased toward the south and east directions where both the freshwater quality and thickness are increased. In contrast, the resistivity of the aquifer layer is decreased toward the northwest (the Mediterranean Sea direction) due to the effect of seawater intrusion.

6 Recommendations

Geoelectrical resistivity was successful for imaging the seawater-freshwater relationship and classifying the aquifer lithology in the target area. Therefore, the results of this work are recommended to be used by the decision makers for groundwater management planning in the study area.

Acknowledgments The authors are grateful to Tanta University for the financial support offered during the course of this research work. The authors thank the editor Prof. Dr. Abdelazim Negm for his constructive remarks.

References

1. Satriani A, Loperte A, Imbrenda V, Lapenna V (2012) Geoelectrical surveys for characterization of the coastal saltwater intrusion in metapontum forest reserve (Southern Italy). *Int J Geophys*. <https://doi.org/10.1155/2012/238478>
2. Post VEA (2005) Fresh and saline groundwater interaction in coastal aquifers: is our technology ready for the problems ahead. *Hydrogeol J* 13:120–123
3. Salem ZE, Al Temamy AM, Salah MK, Kassab M (2016) Origin and characteristics of brackish groundwater in Abu Madi coastal area, Northern Nile Delta, Egypt. *Estuar Coast Shelf Sci* 178:21–35
4. Sherif MM, Kacimov A (2007) Seawater intrusion in the coastal aquifer of Wadi Ham, UAE: a new focus on groundwater seawater interactions. *Proceedings of symposium HS 1001 at IUGG 2007, Perugia, vol 312. IAHS, Wallingford*, pp 315–325
5. Wilson J, Townley LR, Sa Da Costa A (1979) Mathematical development and verification of a finite element aquifer flow model AQUIFEM-1, technology adaptation program, Report No. 79-2. M.I.T., Massachusetts
6. Diab MS, Saleh MF (1982) The hydrogeochemistry of the pleistocene aquifer, Nile Delta area, Egypt. *Environmental International, Alex*, pp 75–85
7. Sherif MM, Singh VP, Amer AM (1988) A two-dimensional finite element model for dispersion (2D-FED) in coastal aquifer. *J Hydrol* 103:11–36
8. Sherif MM, Singh VP, Amer AM (1990) A note on saltwater intrusion in coastal aquifers. *J Water Resour Manag* 4:113–123
9. Sherif MM, Sefelnasr A, Javadi A (2012) Incorporating the concept of equivalent freshwater head in successive horizontal simulations of seawater intrusion in the Nile Delta Aquifer. *Egypt. J Hydrol* 464-465:186–198. <https://doi.org/10.1016/j.jhydrol.2012.07.007>
10. Diab MS, Dahab K, El Fakharany M (1997) Impacts of the paleohydrological conditions on the groundwater quality in the northern part of Nile Delta. *The geological society of Egypt, Cairo. J Geol* 4112B:779–795
11. Petalas CP, Diamantis IB (1999) Origin and distribution of saline groundwaters in the upper Miocene aquifer system, coastal Rhodope area, northeastern Greece. *Hydrogeol J* 7:305–316
12. Sherif MM (1999) The Nile delta aquifer in Egypt. In: Bear J et al (eds) *Seawater intrusion in coastal aquifers: concepts, methods and practices. Theory and application of transport in porous media, vol 14. Kluwer Academic, Dordrecht*, pp 559–590
13. Polemio M, Limoni PP, Mitolo D, Santaloia F (2002) Characterisation of the Ionian-Lucanian coastal aquifer and seawater intrusion hazard. In: *Proceedings of the 17th salt water intrusion meeting, Delft*, pp 422–434

14. Petalas C, Lambrakis N (2006) Simulation of intense salinization phenomena in coastal aquifers-the case of the coastal aquifers of Thrace. *J Hydrol* 324:51–64
15. Somay MA, Gemicci U (2009) Assessment of the salinization process at the coastal area with hydrogeochemical tools and geographical information systems (GIS): Selçuk plain, Izmir, Turkey. *Water Air Soil Pollut* 201:55–74
16. Salem ZE, Gaame OM, Hassan TM (2008) Using temperature logs and hydrochemistry as indicators for seawater intrusion and flow lines of groundwater in the Quaternary aquifer, Nile Delta, Egypt. In: *Proceeding of the 5th international symposium on geophysics*, Tanta, pp 25–38
17. Salem ZE, El-Horiny MM (2014) Hydrogeochemical evaluation of calcareous eolianite aquifer with saline soil in a semiarid area. *Environ Sci Pollut Res* 21:8294–8314
18. Sefelnasr A, Sherif MM (2014) Impacts of seawater rise on seawater intrusion in the Nile Delta aquifer, Egypt. *Ground Water* 52:264–276
19. Salem ZE, Osman OM (2017) Use of major ions to evaluate the hydrogeochemistry of groundwater influenced by reclamation and seawater intrusion, West Nile Delta, Egypt. *Environ Sci Pollut Res* 24:3675–3704. <https://doi.org/10.1007/s11356-016-8056-4>
20. Werner AD, Bakker M, Post VEA, Vandenbohede A, Lu C, Ataie-Ashtiani B, Simmons CT, Barry DA (2013) Seawater intrusion processes, investigation and management: recent advances and future challenges. *Adv Water Resour* 51:3–26
21. Choudhury K, Saha DK, Chakraborty P (2001) Geophysical study for saline water intrusion in a coastal alluvial terrain. *J Appl Geophys* 46:189–200
22. Mailliet GM, Rizzo E, Revil A, Vella C (2005) High resolution electrical resistivity tomography (ERT) in a transition zone environment: application for detailed internal architecture and infilling processes study of a Rhône River paleo-channel. *Mar Geophys Res* 26:317–328
23. Gurunadha Rao VVS, Tamma Rao G, Surinaidu L, Rajesh R, Mahesh J (2011) Geophysical and geochemical approach for seawater intrusion assessment in the Godavari Delta Basin, India. *Water Air Soil Pollut* 217:503–514
24. Steeples DW (2001) Engineering and environmental geophysics at the millennium. *Geophysics* 66:31–35
25. Lapenna V, Lorenzo P, Perrone A, Piscitelli S, Rizzo E, Sdao F (2005) 2D electrical resistivity imaging of some complex landslides in the Lucanian Apennine chain, southern Italy. *Geophysics* 70:11–18
26. Pantelis S, Kouli M, Vallianatos F, Vafidis A, Stavroulakis G (2007) Estimation of aquifer hydraulic parameters from surficial geophysical methods: a case study of Keritis Basin in Chania (Crete – Greece). *J Hydrol* 338:122–131
27. Chianese D, Lapenna V (2007) Magnetic probability tomography for environmental purposes: test measurements and field applications. *J Geophys Eng* 4:63–74
28. Naudet V, Lazzari M, Perrone A, Loperte A, Piscitelli S, Lapenna V (2008) Integrated geophysical and geomorphological approach to investigate the snowmelt-triggered landslide of Bosco Piccolo village (Basilicata, southern Italy). *Eng Geol* 98:156–167
29. Urish DW, Frohlich RK (1990) Surface electrical resistivity in coastal groundwater exploration. *Geoexploration* 26:267–289
30. Ebraheem AAM, Senosy MM, Dahab KA (1997) Geoelectrical and hydrogeochemical studies for delineating ground-water contamination due to salt-water intrusion in the northern part of the Nile Delta, Egypt. *Ground Water* 35:216–222
31. Kruse SE, Brudzinski MR, Geib TL (1998) Use of electrical and electromagnetic techniques to map seawater intrusion near the Cross-Florida Barge Canal. *Environ Eng Geosci* 4:331–340
32. Nowroozi AA, Horrocks SB, Henderson P (1999) Saltwater intrusion into the freshwater aquifer in the eastern shore of Virginia: a reconnaissance electrical resistivity survey. *J Appl Geophys* 42:1–22
33. Abdul Nassir SS, Loke MH, Lee CY, Nawawi MNM (2000) Salt-water intrusion mapping by geoelectrical imaging surveys. *Geophys Prospect* 48:647–661

34. Balia R, Gavaudò E, Ardaù F, Ghiglieri G (2003) Geophysical approach to the environmental study of a coastal plain. *Geophysics* 68:1446–1459
35. Choudhury K, Saha DK (2004) Integrated geophysical and chemical study of saline water intrusion. *Ground Water* 42:671–677
36. Batayneh AT (2006) Use of electrical resistivity methods for detecting subsurface fresh and saline water and delineating their interfacial configuration: a case study of the eastern Dead Sea coastal aquifers, Jordan. *Hydrogeol J* 14:1277–1283
37. Bauer P, Supper R, Zimmermann S, Kinzelbach W (2006) Geoelectrical imaging of groundwater salinization in the Okavango Delta, Botswana. *J Appl Geophys* 60:126–141
38. Khalil MH (2006) Geoelectric resistivity sounding for delineating salt water intrusion in the Abu Zenima area, west Sinai. *Egypt. J Geophys Eng* 3:243–251
39. Sherif M, El Mahmoudi A, Garamoon H, Kacimov A (2006) Geoelectrical and hydro-geochemical studies for delineating seawater intrusion in the outlet of Wadi Ham, UAE. *Environ Geol* 49:536–551
40. Koukadaki MA, Karatzas GP, Papadopoulou MP, Vafidis A (2007) Identification of the saline zone in a coastal aquifer using electrical tomography data and simulation. *Water Resour Manag* 21:1881–1898
41. Cimino A, Cosentino C, Oieni A, Tranchina L (2008) A geophysical and geochemical approach for seawater intrusion assessment in the Acquedolci coastal aquifer (Northern Sicily). *Environ Geol* 55:1473–1482
42. Fadili A, Najib S, Mehdi K, Riss J, Malaurent P, Makan A (2017) Geoelectrical and hydro-chemical study for the assessment of seawater intrusion evolution in coastal aquifers of Oualidia, Morocco. *J Appl Geophys* 146:178–187
43. Salem ZE (2009) Natural and human impacts on the groundwater under an Egyptian village, central Nile Delta: a case study of Mehallet Menouf. In: 13th international water technology conference (IWTC, 13), Hurghada, 12–15 Mar 2009, vol 3, pp 1397–1414
44. Attwa M, Basokur A, Akca I (2014) Hydraulic conductivity estimation using direct current (DC) sounding data: a case study in East Nile Delta, Egypt. *Hydrogeol J* 22:1163–1178. <https://doi.org/10.1007/s10040-014-1107-3>
45. Gemal K, El-Shishtawy AM, El-Alfy M, Ghoneim MF, El-Bary MHA (2011) Assessment of aquifer vulnerability to industrial waste water using resistivity measurements. A case study, along El-Gharbyia main drain, Nile Delta, Egypt. *J Appl Geophys* 75:140–150
46. Kashef A (1983) Salt water intrusion in the Nile Delta. *Groundwater* 21:160–167
47. Mabrouk B, Arafa S, Gemal K (2015) Water management strategy in assessing the water scarcity in Northern Western region of Nile Delta, Egypt. *Geophysical research abstracts*, vol 17. EGU General Assembly 2015, Vienna. EGU2015-15805, 2015
48. McGranahan G, Balk D, Anderson B (2007) The rising tide: assessing the risks of climate change and human settlements in low elevation coastal zones. *Environ Urban* 19:17–37
49. Mabrouk MB, Jonoski A, Solomatine D, Uhlenbrook S (2013) A review of seawater intrusion in the Nile Delta groundwater system – the basis for assessing impacts due to climate changes and water resources development. *Hydrol Earth Syst Sci Discuss* 10:10873–10911. <https://doi.org/10.5194/hessd-10-10873-2013>
50. Attwa M, Gemal KS, Eleraki M (2016) Use of salinity and resistivity measurements to study the coastal aquifer salinization in a semi-arid region: a case study in northeast Nile Delta, Egypt. *Environ Earth Sci* 75:784
51. Mohamed AK (2016) Application of DC resistivity method for groundwater investigation, case study at West Nile Delta, Egypt. *Arab J Geosci* 9:11
52. Tarabees E, El-Qady G (2016) Sea water intrusion modeling in Rashid area of Nile Delta (Egypt) via the inversion of DC resistivity data. *Am J Clim Chang* 5:147–156. <https://doi.org/10.4236/ajcc.2016.52014>
53. Salem ZE, Osman MO (2016) Shallow subsurface temperature in the environs of El-Nubaria canal, northwestern Nile Delta of Egypt: implications for monitoring groundwater flow system. *Environ Earth Sci* 75:1241. <https://doi.org/10.1007/s12665-016-6046-y>

54. Salem ZE, Atwia MG, El-Horiny MM (2015) Hydrogeochemical analysis and evaluation of groundwater in the reclaimed small basin of Abu Mina, Egypt. *Hydrogeol J.* <https://doi.org/10.1007/s10040-015-1303-9>
55. Fadlelmawla AA, Dawoud MA (2006) An approach for delineating drinking water wellhead protection areas at the Nile Delta, Egypt. *J Environ Manag* 79:140–149
56. El-Bayumy DA (2014) Sedimentological and hydrological studies on the area west of the Nile Delta, Egypt. MSc thesis, Tanta University
57. Salem ZE, El Bayumy DA (2016a) Hydrogeological, petrophysical and hydrogeochemical characteristics of the groundwater aquifers east of Wadi El-Natron, Egypt. *NRIAG J Astron Geophys* 5:106–123
58. Salem ZE, El Bayumy DA (2016b) Use of the subsurface thermal regime as a groundwater-flow tracer in the semi-arid western Nile Delta, Egypt. *Hydrogeol J* 24:1001–1014. <https://doi.org/10.1007/s10040-016-1377-z>
59. Osman OM (2014) Hydrogeological and geoenviromental studies of El Behira Governorate, Egypt. PhD dissertation, Tanta University
60. El Shazly EM, Abdel-Hady M A, El-Ghawab MA, El Kassas IA, Khawasil SM, El Shazly MM, Sanad S (1975) Geological interpretation of Landsat Satellite Images for west Nile Delta area, Egypt. Remote Sensing Research project. Academy of Scientific Research Technology, Cairo
61. El Ghazawi MM (1982) Geological studies of the Quaternary-Neogene aquifers in the area northwest Nile Delta. MSc thesis, Al-Azhar University
62. Mabrouk MA (1978) Electrical prospecting on the groundwater in the area west of Cairo-Alexandria desert road (between Wadi El- Natron and El-Nasr Canal). MSc thesis, Faculty of Science, Ain Shams University
63. Abdel Wahab S (1999) Hydrogeological and isotope assessment of groundwater in Wadi El-Natron and Sadat city, Egypt. MSc thesis, Faculty of Science, Ain Shams University
64. Saad K (1962) Groundwater studies of Wadi El-Natron and its vicinities. Desert Institute, Cairo, p 61
65. Desert Research Institute (DRI) (1974) Report on the regional hydrogeological studies of the West El Nubaria area (300,000 Feddans reclamation project), internal report, Cairo, 125 p
66. Abdel Baki AA (1983) Hydrogeological and hydrochemical studies on the area west of Rosette branch and south of El-Nasr Canal. PhD thesis, Faculty of Science, Ain Shams University
67. Milsom J (2003) Field geophysics, 3rd edn. Wiley, Chichester, p 247
68. Palacky GJ (1987) Resistivity characteristics of geologic targets. In: Nabighian MN (ed) *Electromagnetic methods in applied geophysics theory*, vol 1. Society of Exploration Geophysicists, Tulsa, Okla, pp 53–129
69. Bobachev AA, Modin IN, Chevnin VA (2001) IPI2win v. 2.0: user's guide. Moscow State University, Geological Faculty, Department of Geophysics, Moscow, p 35
70. Rockwork (2004) Earth Science and GIS Software (Geosof), www.rockware.com. Suite 101 Golden, CO 80401 USA